BNL-224757-2023-JAAM

GRP-COCA-20

Microscopic Investigation of H2 Reduced CuOx/Cu(111) and ZnO/CuOx/Cu(111) Inverse Catalysts: STM, AP-XPS, and DFT Studies

V. Mehar, J. A. Rodriguez

To be published in "ACS Catalysis"

July 2023

Chemistry Department

Brookhaven National Laboratory

U.S. Department of Energy

USDOE Office of Science (SC), Basic Energy Sciences (BES) (SC-22)

DISCLAIMER

Microscopic investigation of H_2 reduced CuO_x/Cu(111) and ZnO/CuO_x/Cu(111) inverse catalysts: STM, AP-XPS and DFT studies

Vikram Mehar[1], Erwei Huang[1], Rui Shi[2], Ning Rui[1], Rina Rosales[2], Iradwikanari Waluyo[3], Adrian Hunt[3], Ping Liu[1,2] and José A. Rodriguez*[,1,2]

[1]Chemistry Department, Brookhaven National Laboratory, Upton, New York 11973 (USA)

[2]Department of Chemistry, Stony Brook University, Stony Brook, New York 11794 (USA)

[3]National Synchrotron Light Source II, Brookhaven National Laboratory, Upton, New York 11973 (USA)

*To whom correspondence should be addressed, rodrigez@bnl.gov

Tel. 631-344-2246

Abstract

Understanding the reduction mechanism of CuO_x-ZnO interfaces by hydrogen is of great importance for advancing the performance of industrial catalysts for CO_2 hydrogenation to methanol. Here, the reduction of pristine and ZnO-modified CuO_x/Cu(111) by H_2 was investigated using ambient pressure scanning tunnelling microscopy (AP-STM), ambient pressure X-ray photoelectron spectroscopy (AP-XPS) and density functional theory (DFT). The morphological changes and reaction rates seen for the reduction of CuO_x/Cu(111) and ZnO/CuOx/Cu(111) are very different. On CuO_x/Cu(111), perfect "44" and "29" structures displayed a very low reactivity towards H_2 at room temperature. A long induction period associated with an autocatalytic process was observed to enable the reduction by the removal of chemisorbed non-lattice oxygen initially and lattice oxygen sequentially at the CuO_x-Cu interface, which led to formation of oxygen deficient "5-7" hex and honeycomb structures. In the final stages of the reduction process, regions of residual oxygen species and metallic Cu were seen. The addition of ZnO particles to CuO_x/Cu(111) opened new reaction channels. On the ZnO sites, the dissociation of H_2 was fast and H adatoms easily migrated to adjacent regions of copper oxide. This hydrogen spillover substantially enhanced the rate of oxygen removal, resulting in the rapid reduction of the copper oxide located in the periphery of the zinc oxide islands with no signs for the reduction of ZnO. The deposited ZnO completely modified the dynamics for H_2 dissociation and hydrogen migration, providing an excellent source for CO_2 hydrogenation processes on the inverse oxide/metal system.

Keywords: H_2 activation, H spillover, CO_2 hydrogenation, inverse ZnO/Cu catalysts, morphological studies

Introduction

Climate change is one of the major concerns of the 21st century. Greenhouse gases like CO_2, NO_2 and CH_4 are major contributors to climate change, with CO_2 being the worse pollutant[1]. In our age of massive industrialization, the mitigation measures to control CO_2 emissions have been limited. Therefore, there is an ever increasing need to capture and convert CO_2 into value added species. Copper and copper oxide-based catalysts have been widely used in C1 processes that are linked to the conversion of CO_2[2-9]. Cu_2O possesses photovoltaic and photocatalytic properties as well. H_2 can act as a green fuel as the demand for energy increases and the fossil fuels stocks deplete. One of the ways in which CO_2 could be utilized is by hydrogenation to produce methanol (CH_3OH). Traditionally, the CO_2 hydrogenation is done on zinc – copper oxide-based catalysts dispersed on a silicon oxide or alumina support[2-6]. A study of high-resolution transmission electron microscopy (HR-TEM) has shown that the active phase of industrial $Cu/ZnO/Al_2O_3$ catalysts consists of a layer of graphitic ZnO on top of the copper surface[3]. The reconstruction of the catalysts into an inverse oxide/metal configuration has a strong effect on their performance[5].

A good knowledge of the microscopic phenomena associated with the dissociation of H_2 and the reduction of copper oxides and $ZnO\text{-}CuO_x$ interfaces is essential for optimizing the $CO_2 \rightarrow CH_3OH$ conversion and other catalytic processes where hydrogen plays a vital role such as the water-gas shift reaction and the hydrogenation of unsaturated organic hydrocarbons[7, 8, 10]. The microscopic (or atomic) mechanism for the reduction of $ZnO\text{-}CuO_x$ interfaces by H_2 is unknown. Previous studies have only dealt with the atomic details associated with the reduction of surfaces of copper oxides[9-15]. Time-resolved X-ray diffraction and X-ray absorption fine structure have been used to investigate the reduction of powders of CuO and Cu_2O with H_2[11-13]. The reduction of CuO was found to be much easier than the reduction of Cu_2O. The reduction mechanism involved

induction times and the embedding of H atoms in the lattice of the copper oxides[11, 12]. The reduction rates for the CuO → Cu_2O and Cu_2O → Cu transformations crucially depended on the initial concentration of defects on the oxide surfaces. In general, the formation of the product phase (either Cu_2O or Cu) was triggered once a certain density of accumulated oxygen vacancies was reached at the periphery of the parent phase (either CuO or Cu_2O)[11, 13]. Moreover, the O-deficient Cu_2O can form a stable intermediate before the Cu_2O is fully reduced to metallic Cu. Many of these findings have been verified in subsequent studies involving transmission electron microscopy (TEM) or scanning tunneling microscopy (STM)[14-16]. The results of calculations based on density-functional theory (DFT) indicate that when one H_2 molecule is placed on the top of surface O, the H_2 molecule dissociates spontaneously into two H atoms that bond with the adjacent lattice O to form two hydroxyls[15, 17]. Eventually hydrogen adsorption leads to the formation of H_2O that evolves spontaneously from the surface leaving behind a reduced oxide. The combined process of H_2 dissociation and H_2O formation is accelerated by the presence of defects or dislocations in the copper oxide[15-17]. These findings are important for understanding the role of defect stability on the lifetime of transient structures seen in the reduction mechanisms.

As mentioned above, the possibility of using oxide-oxide interfaces opens an exciting opportunity for creating active sites for CO_2 conversion and C1 catalysis in general [3, 5, 18-23]. For instance, interfaces generated by the deposition of nanoparticles of ZnO, CeO_2, SnO_2 or ZrO_2 on a copper oxide substrate can be very active in the hydrogenation of CO_2 to methanol[4, 18-22]. Indeed, an industrial $Cu/ZnO/Al_2O_3$ powder catalyst adopts an inverse ZnO/Cu configuration during methanol synthesis[2]. Here, we focus our attention on how the addition of ZnO nanoparticles can affect interactions with H_2 and the reduction of copper oxide. Theoretical studies by Nyberg et. al predict that corner sites of ZnO are favored for H_2 dissociation generating a metal hydride and

hydroxyl species[24]. DFT + U calculations by Pacchioni and coworkers predict heterolytic cleavage for H_2 adsorbed on wurtzite ZnO and a homolytic cleavage on bilayer ZnO supported on coinage metals[25]. Mun and coworkers also studied H_2 adsorption on ZnO(0001) utilizing ambient-pressure X-ray photoelectron spectroscopy (AP-XPS) and they found that H_2 dissociation results in the formation of hydroxyl species that prefers to go subsurface inside the ZnO lattice[26]. In general, the dissociation mechanism of H_2 on CuO_x-ZnO, or other type of copper-metal oxide interface, is not well understood largely due to the difficulty in preparing well defined surfaces for controlled investigation. The lack of experimental data and the difficulty in obtaining microscopic details warrants the current study.

In this work, a combination of scanning tunneling microscopy (STM), AP-XPS and calculations based on density functional theory (DFT) is employed to study and compare the reduction of CuO_x/Cu(111)[27-29] and ZnO/CuO_x/Cu(111)[30] systems. We pay particular attention to the induction time for copper oxide reduction and how this is affected by the addition of ZnO to the surface. Well-ordered surfaces of defective CuO_x were prepared by exposing Cu(111) to O_2 at elevated temperatures (600 - 700 K)[27-29]. The density of O vacancies and defects in these oxide overlayers was controlled by manipulating the background O_2 pressure and the temperature of copper oxidation[27-29]. Large islands of ZnO (300 - 500 nm in size) were prepared on the CuO_x/Cu(111) surfaces by vapor depositing Zn under an O_2 background at 600 K[30]. Our results show big differences in the mechanisms for CuO_x/Cu(111) and ZnO/CuO_x/Cu(111) reduction. H_2 dissociation and H spillover are facile on ZnO_x islands and play a vital role in mediating chemical transformations on the ZnO-CuO_x interface.

Experimental Details

A. Studies of scanning tunneling microscopy

Scanning tunneling microscopy (STM) measurements were performed in an ultrahigh vacuum (UHV) system with a base pressure of 5 x 10^{-10} Torr. The UHV chamber is equipped with a scanning tunnelling microscope, a quadrupole mass spectrometer, an ion sputter gun and a three-pocket electron beam evaporator. The equipment used for scanning tunnelling microscopy was produced by SPECS Aarhus. It can operate at variable temperature and near ambient pressure conditions. The STM is housed in a cell that could be pressurized to near ambient pressure with the help of locking screws that keep the chamber under UHV.

The Cu(111) crystal used in this study is a circular disc shaped (8 mm x 2 mm) cut to isolate the (111) surface plane within a tolerance of $\pm 0.1^0$. The sample was heated using radiative and e-beam heating. A type-K thermocouple attached to the bottom of the sample was used to monitor the sample temperature. Sample cleaning consisted of cycles of sputtering with 2000 eV Ar^+ ions at a surface temperature of 300 K, followed by annealing at 800 K in UHV. A thin copper oxide film was grown by exposing the Cu(111) surface to 5 x 10^{-7} Torr molecular oxygen at 600 K for 15 min followed by cooling in oxygen background for 10 min. Zinc oxide islands were grown on pristine copper oxide by vapor depositing zinc in 5 x 10^{-7} Torr O_2 at 600 K. H_2 was dosed in a high pressure cell which was held with locking screws. The CuO_x/Cu(111) and ZnO/CuO_x/Cu(111) surfaces were exposed to 50 mTorr of H_2 at 300 K and the evolution of their morphologies was followed as a function of time. STM images were scanned in UHV after evacuating H_2 from the chamber. A commercially etched tungsten tip was used for scanning and the images were collected under constant current mode.

B. Studies of ambient-pressure XPS

The ambient pressure X-ray photoelectron spectroscopy (AP-XPS) experiments were performed in two separate chambers. AP-XPS experiments for H_2 reduction on pristine

CuO_x/Cu(111) were performed at beamline 23-ID-2 (IOS) of the National Synchrotron Light Source II (NSLS-II) at Brookhaven National Laboratory (BNL), with the specification of this beamline and end station reported previously[31-33]. The procedure for cleaning Cu(111) and growth of copper oxide was similar to the procedures described in the earlier sections. The CuO_x/Cu(111) was exposed to 50 and 200 mTorr of H_2 at 300 K. The binding energy scale was calibrated to the Cu 3p peak at 75 eV. A photon energy of 720 eV was used to collect O 1s, C 1s and Cu 3p regions. Step size of 0.1 eV was used to collect the O 1s data and the overall energy resolution in the spectra was ~ 0.1 eV. CasaXPS software was used for data analysis. A Shirley-type background subtraction was performed for the O 1s spectra and the peaks were fitted with GL(30) functions. The AP-XPS experiments on ZnO/CuO_x/Cu(111) were performed in a commercial SPECS AP-XPS chamber equipped with a PHOIBOS 150 EP MCD-9 analyzer at the Chemistry Division of BNL. The procedure for cleaning Cu(111) and the growth of ZnO/CuO_x/Cu(111) is described in the previous section[30, 34, 35]. The spectra were collected in a constant H_2 background pressure of 50 mTorr at 300 K

C. Studies of density functional theory

All the calculations were performed with spin-polarized density functional theory (DFT)[36] by Vienna Ab Initio Simulation Package (VASP)[37]. The projector augmented wave method (PAW)[38] together with GGA exchange correlation functional with the PBE functional[39] were employed with a 400 eV kinetic energy cutoff. Gaussian smearing with a width of 0.05 eV was used to improve the convergence. Monkhorst-Pack[40] meshes with 3×3×1 were used to sample the Brillouin zone for all the surface calculations. The DFT calculated binding energies for H_2 on Cu(111)-based surface were calculated as: ΔE_b = E(H/Surface) – 1/2E(H_2) − E(Surface), where E is the DFT calculated total energy.

In these calculations, the '44-structure' model was constructed with 3 layers of 4×4 Cu(111) surface and one monolayer of $CuO_{0.88}$ with the employment of Hubbard U[41] (U_{eff} = 5.2) for highly correlated Cu 3d electrons, according to our previous work[42-44], (Figure 1c). The '29-structure' model was constructed by putting one layer of $CuO_{0.94}$ on the Cu(111) surface with a √13 R46.1° × 7 R21.8° supercell that was four layers thick (Figure 1d), which has been identified as a structurally accurate model for the '29-structure' by McEwen and Sykes[45, 46]. During the DFT calculations, bottom two layers were fixed while the rest were allowed for fully relaxation for both "44-structure" and "29-structure". Hereafter, the copper oxide comprised of "29" and "44" structure will be referred to as CuO_x for the sake of simplicity.

Three models were used to describe the step sites, defect sites and the terrace sites of $ZnO/CuO_x/Cu(111)$ model catalyst observed by STM following our previous studies[47, 48]. Specifically, step-rich Zn_3O_3 cluster model, O-rich ZnO overlayer and stoichiometric ZnO overlayer were adopted for describing the STM observed coarse $ZnO/CuO_x/Cu(111)$ model surface. "44 structure" $CuO_x/Cu(111)$ model was considered for the case with ZnO deposition in consideration of complexity introduced by including "22 structure" of $CuO_x/Cu(111)$ model. During the DFT calculations, the bottom two copper layers were fixed and the rest layers were allowed for full relaxation.

Results and Discussion

A. Reaction of H_2 with $CuO_x/Cu(111)$ surfaces

A. 1 Initial morphology of CuO_x on Cu(111): STM studies

A single-layer copper oxide structure was prepared by oxidizing Cu(111) with 5 x 10^{-7} Torr oxygen at 600 K for 15 min, followed by cooling in oxygen background for 10 min[27, 35, 49]. This procedure yields large, atomically flat domains of copper oxide ~ 0.2 nm in height and spread on 20 – 30 nm wide terraces as shown in Fig. 1a. A high -resolution STM image (Fig. 1b) shows that the oxide layer is comprised of large domains of "29" structures separated by 2 – 3 rows of "44" oxide with an oxygen coverage of 0.52 ML and 0.51 ML respectively. Besenbacher et. al report that the woods notation for the "44" and "29" structures are [4/-3 3/5] and [9/1 1/5] with respect to (1 x 1) unit vectors rotated at 120^0 to each other[50]. The "29" structure consists of six distorted hexagonal Cu-O rings, where five of them have oxygen occupying the threefold hollow sites of Cu(111), while the "44" structure is comprised of 8 corrugated Cu-O hexagonal rings[28, 51, 52]. Details of the '44' and '29' structures have been previously investigated elsewhere[52]. The knowledge of the initial morphology of CuO_x is very important because defects and imperfections can affect the reaction with H_2[14, 15] and the growth of ZnO islands is affected by the initial morphology of the CuO_x film[30].

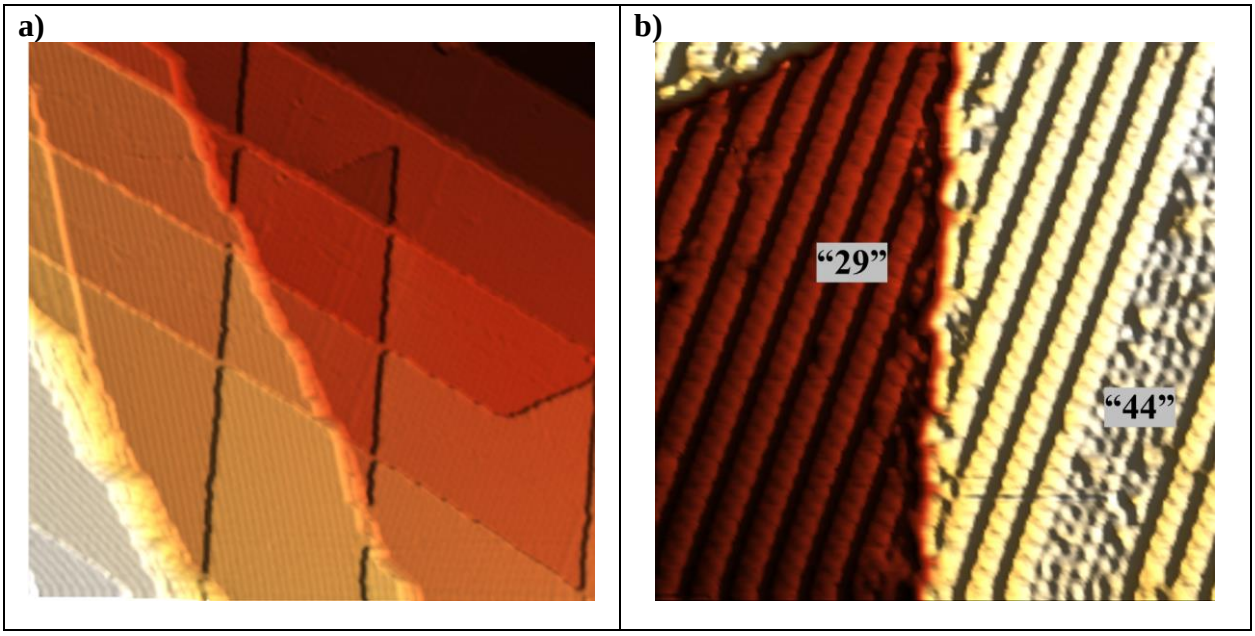

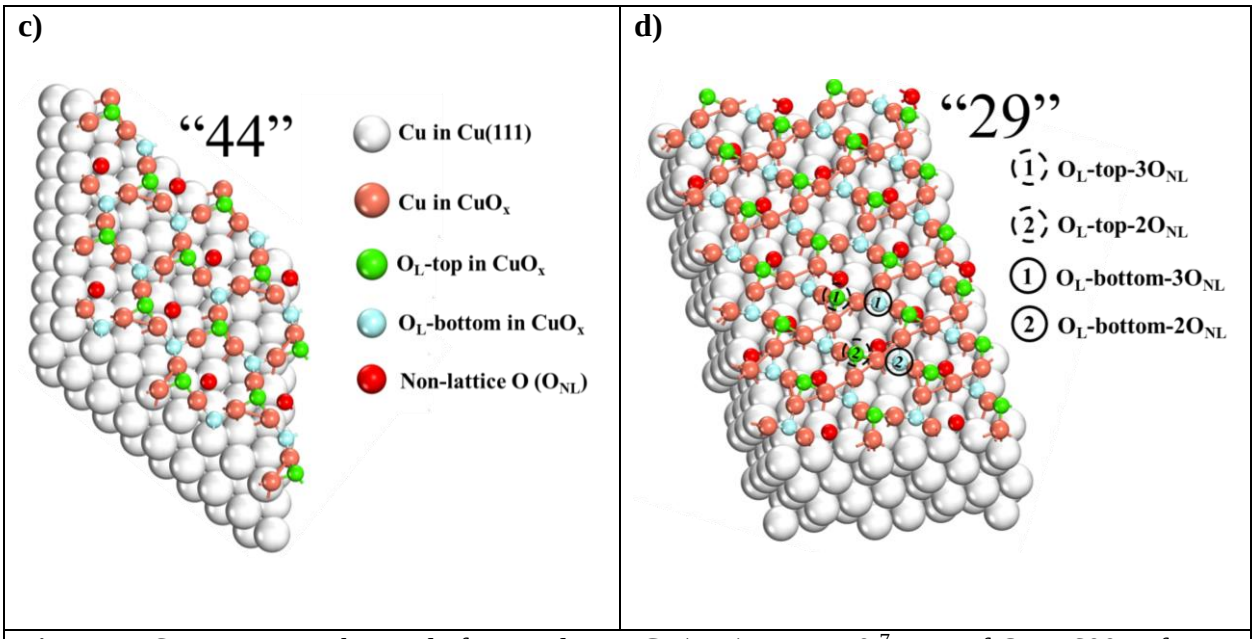

Figure 1: STM images obtained after oxidizing Cu(111) in 5×10^{-7} Torr of O_2 at 600 K for 15 min, followed by cooling in O_2 background for 10 min to generate a CuO_x phase with about 0.52 ML of oxygen. Panel a) 150 nm × 150 nm (500 mV, 0.99 nA) shows large scale morphology and b) 30 nm × 30 nm (354 mV, 0.91 nA) shows a high-resolution image of the "29" and "44" CuO_x structures. Panel c) shows a theoretical model for the '44-structure' of CuO_x/Cu(111); white: Cu in Cu(111) support; copper: Cu in CuO_x layer; green: lattice O at the top of CuO_x layer, cyan: lattice O at the bottom of CuO_x layer; red: non-lattice O, including both fcc and hcp sites. Panel d) shows a theoretical model for the '29-structure' of CuO_x/Cu(111); O_L-top-$3O_{NL}$: lattice O at the top of CuO_x layer, surrounded by three non-lattice O_{NL} hexagonal rings; O_L-top-$2O_{NL}$: lattice O at the top of CuO_x layer, surrounded by two non-lattice O hexagonal rings and one hollow hexagonal ring; O_L-bottom-$3O_{NL}$: lattice O at the bottom of CuO_x layer, surrounded by three non-lattice O hexagonal rings; O_L-top-$2O_{NL}$: lattice O at the bottom of CuO_x layer, surrounded by two non-lattice O hexagonal rings and one hollow hexagonal ring. See Figure S1 and S2 for a detailed top and side view structures.

A.2 Morphology of CuO_x during reduction by H_2: STM Studies

We performed STM experiments to probe the morphology of CuO_x during the initial stages of reduction by H_2. Xu and co-workers conducted a detailed study of in situ reduction of CuO_x with H_2 at 1.64 Torr pressure range[53], however in this work we focus on the details of the very early reduction stages during the induction period using lower H_2 pressure. A single layer CuO_x film

was prepared as described in the previous section. Pristine CuO_x was then exposed to 50 mTorr H_2 at 300 K and the surface was scanned in vacuum after evacuating the H_2. Figure 2 displays the morphology of CuO_x after 1, 2 and 3 hours of cumulative H_2 exposure at a constant pressure of 50 mTorr. One hour of H_2 exposure results in random defects uniformly distributed on the "29" structure mostly arising from the vacancies (Figure 2a). The surface is still mostly covered with the "29" structure while vacancies can be seen distributed randomly along the oxide layer. DFT calculations predict a reduction mechanism where H_2 dissociates onto O atoms to form OH groups that eventually react with hydrogen to form H_2O molecules that desorb leaving behind a reduced oxide[15, 17]. These processes of H_2 dissociation and H_2O formation may have occurred only on a few sites of the surface displayed in Figure 2a. Since the experiments were done at 300 K, one can conclude that on the pristine oxide surface there are significant energy barriers for the cleavage of H-H bonds and the formation of H_2O.

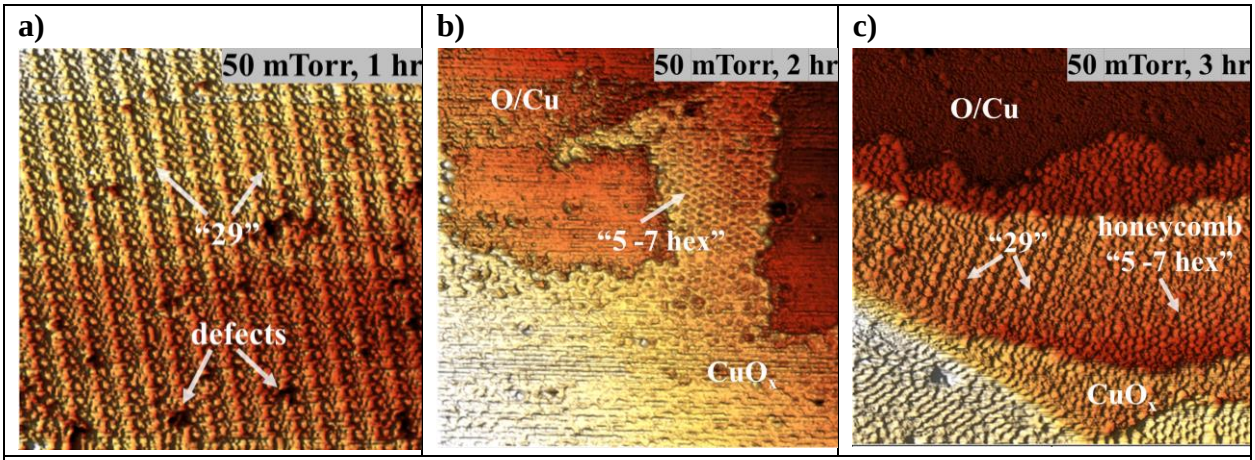

Figure 2: STM images (30 nm x 30 nm) (500 mV, 1 nA) of the CuO_x during a 50 mTorr of H_2 exposure for a cumulative period of (a) 1 hour, (b) 2 hours, and (c) 3 hours at 300 K. H_2 was evacuated from the chamber and the images were collected in a vacuum at room temperature.

Further increasing the H_2 exposure time to 2 hours (Figure 2b) yields a heterogeneous surface comprised of an oxygen-deficient honeycomb-like "5-7" hex structure[27, 35, 49, 52], chemisorbed

oxygen species, as well as Cu metal domains. The acceleration of the reduction rate when going from panel 2a to panel 2b is consistent with the existence of a defect-mediated autocatalytic process as seen in XRD studies for powders and films of copper oxide[9-11]. On the defect sites, the rates for H_2 dissociation and water formation should be fast[15, 17]. In situ STM imaging studies of CuO_x/Cu(111) under 5 x 10^{-8} Torr CO pressure reported oxygen-deficient honeycomb structures and the development of metallic Cu fronts due to a massive mass transfer of Cu atoms on reducing the CuO_x[14, 34, 35, 42, 54]. Xu and coworkers performed an in situ characterization of the reaction of H_2 with CuO_x films and found that the reduction initiates at the step edges and defects sites on the terraces[14]. They report that the formation of metallic Cu fronts begins at the step edges due to the high mobility of Cu atoms that are released from the reduction of CuO_x diffusing across the terraces and joining the nearby Cu step edges[14]. This implies that CuO_x reduction proceeds through stoichiometric oxygen deficient phases before transforming into metal domains in agreement with the previously reported work for CO reduction[27].

In Figure 2c, after a cumulative 3 hours of a large H_2 dose, a segregation between oxygen-rich and metallic domains is apparent. The surface is covered with rough regions of metallic Cu and the boundary is comprised of honeycomb-like oxygen-deficient 5-7 structures. It is possible that H_2 dissociation over undercoordinated copper sites can result in the formation of hydroxyl species near the steps, leading to the formation of ordered oxygen deficient CuO_x. Moreover, the concentric rings, ~ 1 nm in diameter and 0.1 nm in depth, located near the metallic copper domains suggest the formation of chemisorbed oxygen species, indicating a stepwise reduction of CuO_x domains[55]. Overall, our STM results suggests that the reduction of CuO_x by H_2 is a multi-step process involving the formation of hydroxyl species, thereby facilitating the evolution of H_2O gas[15, 17] and causing a slow reduction of the CuO_x domains. Recent XRD measurements by

Unutulmazsoy et al.[13] also show that the reduction of CuO_x in H_2 is preceded by an incubation time during which the oxygen vacancies are accumulated in the oxide subsurface region by H_2O formation and desorption, in agreement with our findings. From our STM studies, we did find that the surface is extremely heterogeneous with some regions comprising of pristine CuO_x domains.

Our data indicates that a major bottleneck for the reduction of CuO_x/Cu(111) is the dissociation of the molecular bond in H_2. As mentioned above, there are some similarities for the reduction of CuO_x with H_2 and CO[42, 53, 54]. Both molecules induce reduction fronts on the copper oxide substrate[42, 53, 54]. However, in the case of reduction by CO, one can bypass the need to dissociate a H-H bond before removing oxygen from the copper oxide. We found a large increase in the rate of CuO_x/Cu(111) reduction when switching from H_2 to CO as the reducing agent. In our instrument, using identical methodologies for the preparation of CuO_x/Cu(111), we found morphologies for CO/CuO_x/Cu(111), shown in Figure 3, never seen for H_2/CuO_x/Cu(111). In the case of CO/CuO_x/Cu(111), the rate of reduction is so fast that the system has no time to rearrange and find the most stable configuration for a given concentration of oxygen. In particular, the STM images collected after exposing 5 mTorr of CO to pristine CuO_x at 300 K reveal the formation of islands of 50 nm in width and 0.18 nm in height as displayed in Figure 3a. Increasing the CO exposure to 20 min results in the growth of these islands such that the metallic copper islands grow at the expense of smaller islands due to Ostwald's ripening and mass transfer of Cu atoms. After a cumulative 30 min of CO exposure, metallic Cu terraces about 0.22 nm is height can be seen, further confirming the Cu mass transfer across the terraces. Initial morphology of CuO_x during exposure to CO at elevated pressures of 10 and 20 mTorr results in the formation of larger islands that are 30 - 100 nm wide, e.g. Figure 3 panel d and g. With increasing CO exposure time, the 10 mTorr and 20 mTorr STM images reveal concentric islands stacked on top of each other formed

from mass transfer of Cu metal atoms from distinct metallic layers. Overall, the morphology of CuO_x after CO exposure showed significant differences compared to H_2-exposed CuO_x. As we will see below, the major bottleneck of dissociating H_2, to produce an enhancement in the rate of copper oxide reduction, also can be accomplished by adding ZnO to the CuO_x/Cu(111) substrate.

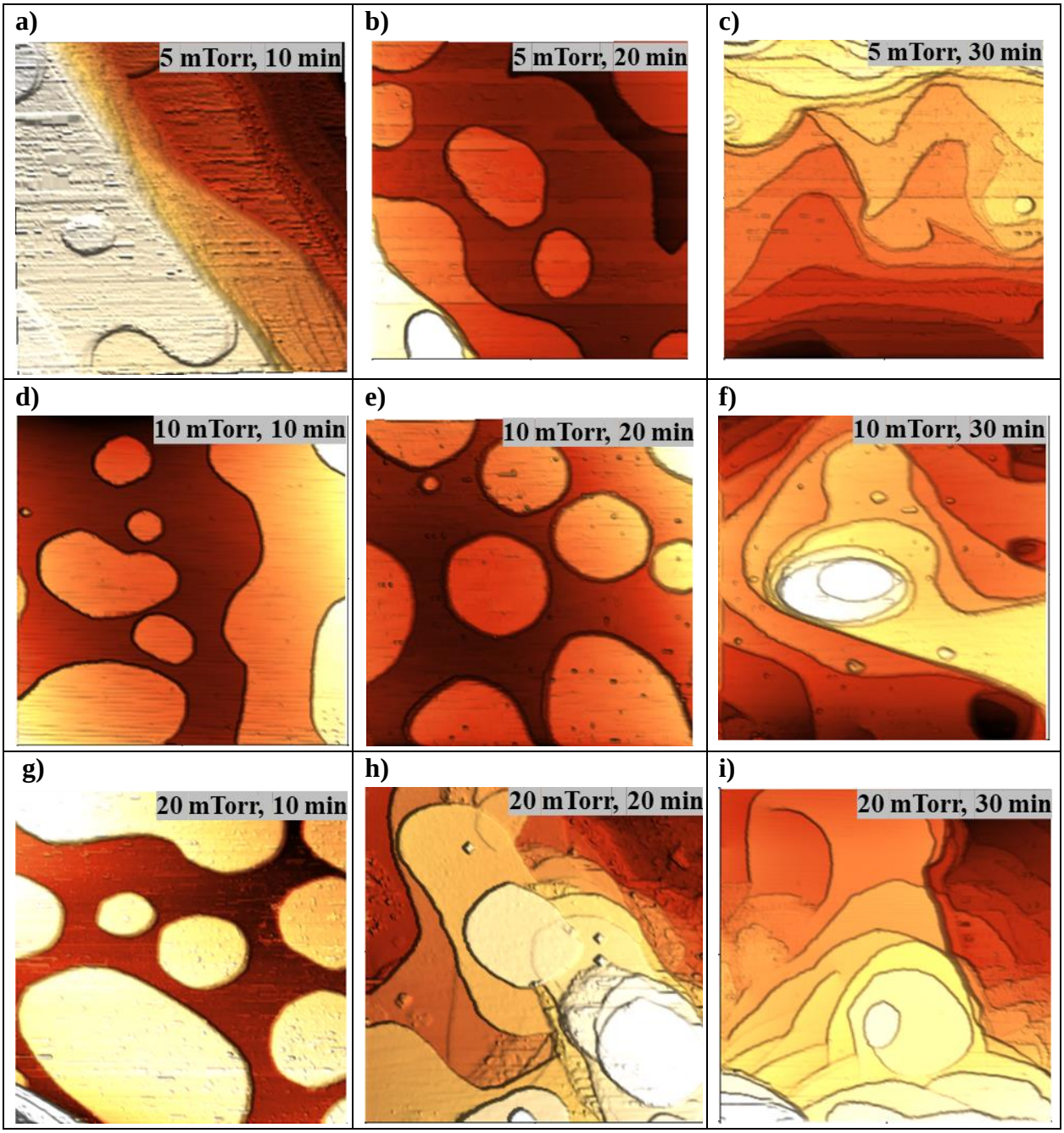

Figure 3: STM images (150 nm x 150 nm) (200 - 500 mV, 0.5 - 1 nA) obtained after reducing pristine CuO_x with 5 mTorr (a-c), 10 mTorr (d-f) and 20 mTorr (g-i) of CO at 300 K. CO was evacuated from the chamber and the images were collected in a vacuum at room temperature.

A.3 Evolution of the chemical state of CuO_x during reduction by H_2: AP-XPS studies

STM experiments shed light on the morphological changes of the CuO_x surface after reduction by H_2. However, to gain further insight into the chemical evolution of these systems, we performed AP-XPS experiments at the IOS (23-ID-2) beamline at NSLS II. Figure 4a and 4b shows the O 1s spectra obtained after exposing pristine CuO_x film to 50 mTorr and 200 mTorr of H_2 at 300 K. Using the high-energy resolution provided by the synchrotron-based AP-XPS studies, we examined the phenomena associated with the induction period of the reduction process. These phenomena have not been studied before at this level of detail.

The high resolution of the O 1s features obtained with the synchrotron light source shows two distinct peaks centered at 529.9 and 529.4 eV. Such a small separation in the binding energies of the O 1s peaks points towards oxygen atoms occupying distinct positions in the CuO_x lattice. Our structural models and those by others show that the "29" and "44" structures of the CuO_x lattice have chemisorbed non-lattice oxygen atoms O_{NL} and oxygen located in the lower layers of copper oxide O_L[52] (see Figure 1 panel c and d). Core level shifts of O 1s also reveal that a difference of 0.5 eV in the binding energy could most likely arise from oxygen species present in different binding environments within the copper oxide lattice[56]. In Figure 4a and 4b, in addition to the peaks for O centers, there are small features for surface OH around 531 eV and a trace for adsorbed H_2O around 532.5 eV[56]. With increasing the H_2 exposure time, the signal for the adsorbed OH and H_2O shows a small increase (~ 15%) as these can be expected as intermediates or products in the reduction process[15, 17]. Their low concentration (< 0.05 monolayer) indicates that H_2 dissociation

and H_2O formation are barely happening. According to previous theoretical calculations[13, 15], a relatively large concentration of surface OH groups is expected when the concentration of defects is large and water dissociation is fast. In Figure 4, the copper oxide surface is at a stage in which the number of defects is small, and the reduction process is very slow (morphology seen in Figure 2a). This is consistent with a previous AP-XPS study also performed at the IOS beamline, where the reduction rate of copper oxide by H_2 was found to be slow over a two-hour period and was only accelerated by the presence of Pt dopants[57].

Figure 4c shows the variation of the O_{NL} and O_L species during the reduction process. Quantitative analysis reveals that the O_L signal decreases by 5 and 10% for 50 and 200 mTorr of 3 hours cumulative H_2 exposure, respectively. However, the O_{NL} intensities dropped by 20% and 46% for 50 mTorr and 200 mTorr H_2 pressure, respectively. This indicates that the non-lattice O_{NL} atoms that are removed in the initial stages of the reduction process come from subsurface layers, which agrees with predictions coming from atomistic simulations and TEM studies for the reduction of CuO films[15]. Our results are consistent with a model in which the onset period involves reaction of H_2 with chemisorbed non-lattice O_{NL} surface atoms to yield water, with a fast migration of O_L from the bulk region to the surface to remove the oxygen vacancy. Eventually, the defects created by this migration accelerate the dissociation of H_2 and make the reduction process autocatalytic[15]. Thus, our STM and AP-XPS results in Figures 2 and 4 indicate that the reduction of copper by H_2 at 300 K is not a spontaneous or fast process.

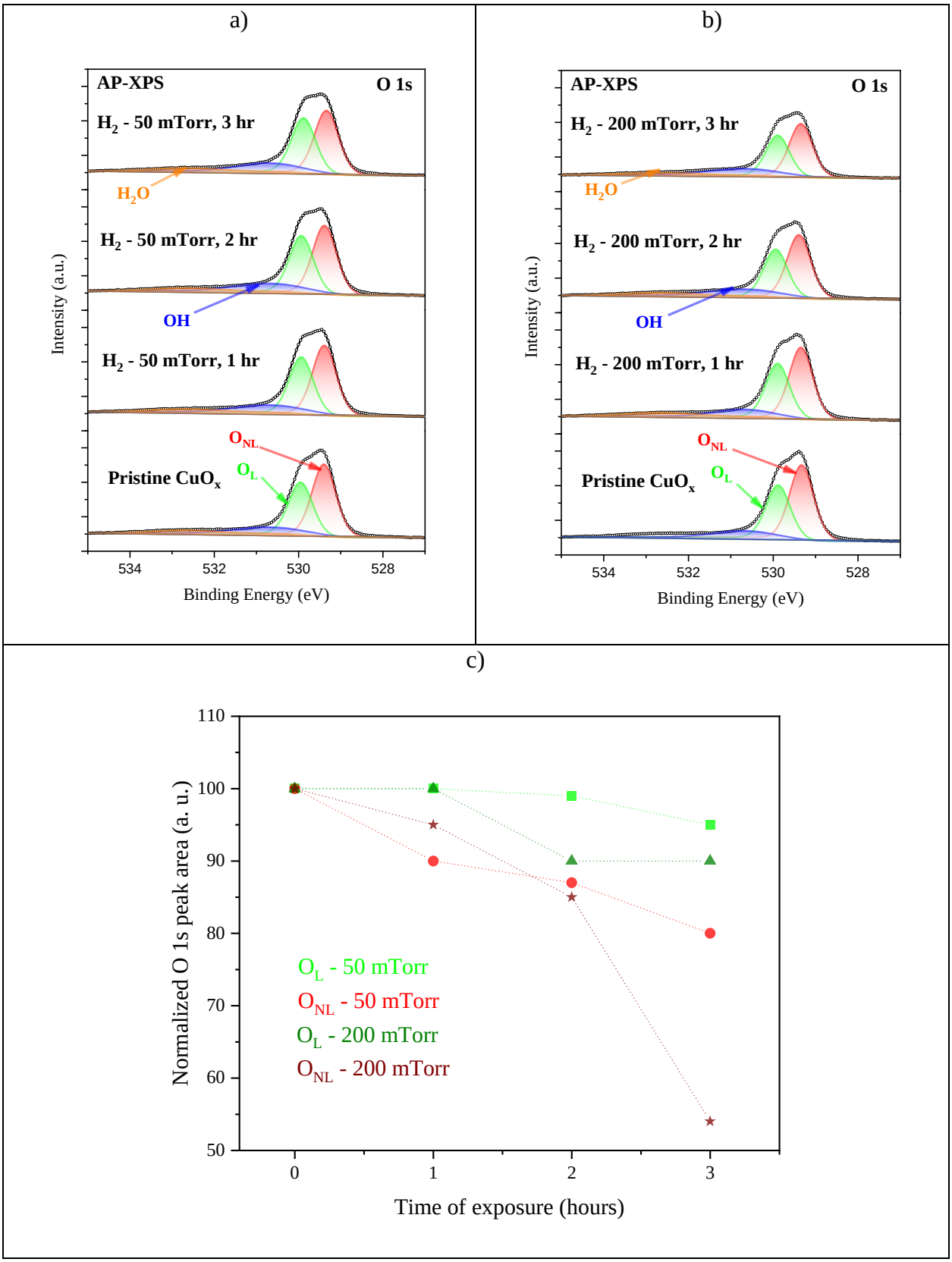
a)
AP-XPS
O 1s
H2 - 50 mTorr, 3 hr
H2O
H2 - 50 mTorr, 2 hr
OH
H2 - 50 mTorr, 1 hr
ONL
OL
Pristine CuOx
Intensity (a.u.)
534
532
530
528
Binding Energy (eV)
b)
AP-XPS
O 1s
H2 - 200 mTorr, 3 hr
H2O
H2 - 200 mTorr, 2 hr
OH
H2 - 200 mTorr, 1 hr
ONL
OL
Pristine CuOx
Intensity (a.u.)
534
532
530
528
Binding Energy (eV)
c)
Normalized O 1s peak area (a. u.)
110
100
90
80
70
60
50
0
1
2
3
Time of exposure (hours)
OL - 50 mTorr
ONL - 50 mTorr
OL - 200 mTorr
ONL - 200 mTorr

Figure 4: O 1s spectra obtained from pristine CuO_x/Cu(111) during H_2 exposure to a) 50 mTorr and b) 200 mTorr at 300 K. Part c: changes in the integrated intensities of O_L and O_{NL} species.

A.4 DFT calculations of H_2 interactions with CuO_x/Cu(111) *catalyst*

DFT calculations were further performed to describe the initial stage of CuO_x/Cu(111) upon the exposure to H_2, and gain better understanding of the corresponding reduction mechanism. Two commonly seen model structures were employed[55], the 44-structure and the 29-structure (e.g. Figure 1c and 1d), and multiple types of chemisorbed non-lattice oxygen (O_{NL}) and lattice oxygen (O_L) sites at the CuO_x-Cu(111) interface were considered for adsorption of dissociated *H fragment. Wherein, O_{NL} was further categorized to O_{NL} at fcc site (O_{NL}-fcc) and hcp site (O_{NL}-hcp) on Cu(111), while O_L was further categorized to O_L at the top of CuO_x layer (O_L-top) and O_L at the bottom (O_L-bottom) of the CuO_x layer for both 44- and 29-structure models. In addition, due to the complexity of the 29-structure model, two different types of top and bottom O_L were studied: O_L-top-3O_{NL} and O_L-top-2O_{NL}, O_L-bottom-3O_{NL} and O_L-bottom-2O_{NL} depending for three and two O_{NL} involved in its corresponding surrounding copper oxide rings.

DFT calculations showed that the O_{NL} sites can provide a stronger binding to hydrogen (binding energy, ΔE_b: -0.64 to -0.74 eV) than the O_L sites (ΔE_b: -0.39 to -0.54 eV). Wherein, the O_{NL}-hcp site (ΔE_b: -0.74 eV for 29-structre; -0.67 eV for 44-structure) is slightly more active than the O_{NL}-fcc site (ΔE_b: -0.66 eV for 29-structre; -0.64 eV for 44-structure), and so do the O_{NL} sites (ΔE_b: -0.66 eV to -0.74 eV in 29-structure as compared to that (ΔE_b: -0.64 eV to -0.67 eV) in to the 44-structure and -(SI Table S1 and Figure 5). Thus, thermodynamically on exposure to hydrogen, the O_{NL} sites in both 44- and 29-structures of CuO_x/Cu(111) likely are active over the O_L sites by preferentially capture *H species and are eventually removed in the form of H_2O. This

is in good agreement with the AP-XPS analysis (Figure 4C). Similar sequence was also observed for the reduction of 44-structure by CO[42].

The O_L-top site in the 29-structure shows a stronger binding capability (binding energy: -0.52 to -0.54 eV) than the one in the 44-structure (ΔE_b: -0.39 eV). By comparison, the behavior of O_L-bottom is more complex, where the binding of *H tends to raise the O_L-bottom outward the surface, which results in significant structural distortion. The O_L-bottom site in the "44"-structure demonstrates a slightly weaker binding to *H than the O_L-top site (difference in binding energy: ~ 0.06 eV). While in the case of 29-structure, the weakening going from the O_L-top site, e.g. O_L-top-$3O_{NL}$, to O_L-bottom site, O_L-bottom-$2O_{NL}$, can be more significant (difference in ΔE_b: ~ 0.32 eV), which is associated with the more prominent structural distortion than that of the "44"-structure during *H adsorption. Yet, the O_L-bottom-$3O_{NL}$ site (ΔE_b: -0.49 eV) in 29-structure can still bind *H more strongly than the O_L-bottom site (ΔE_b: -0.33 eV) in 44-structure. Note the O_L-bottom-$2O_{NL}$ site provides the least binding to *H among the oxygen sites considered, which may be stable enough to survive even in the final stage of reduction. Nevertheless, as demonstrated below, CuO_x/Cu(111) is much less active than ZnO/CuO_x/Cu(111) on exposure to H_2.

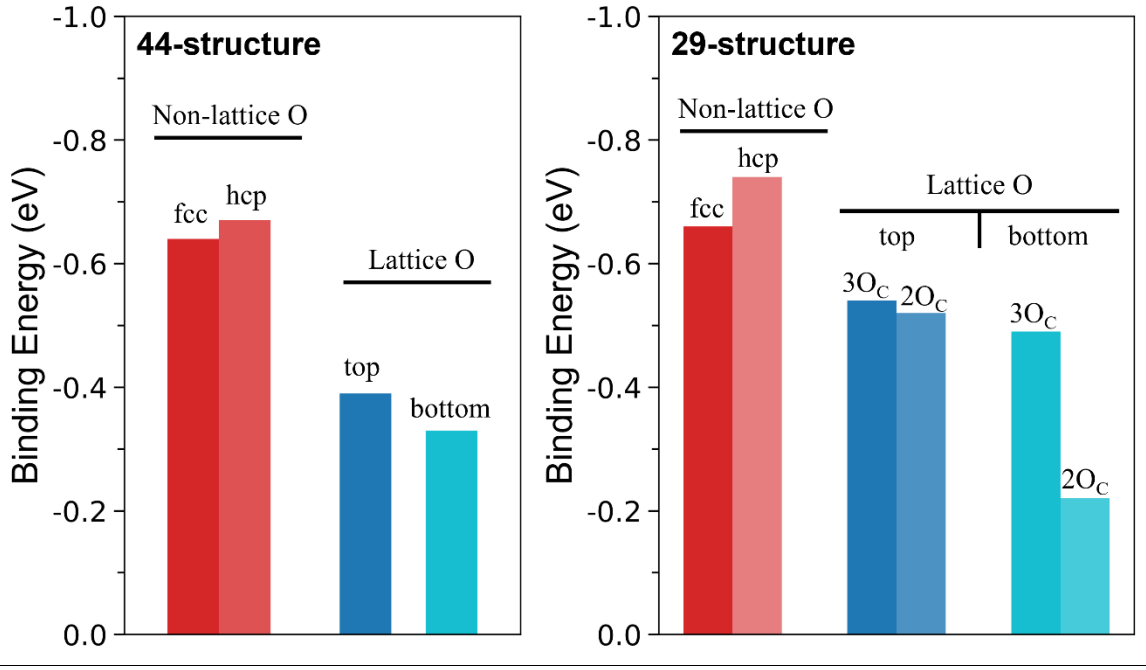

Figure 5: DFT calculated binding energy (ΔE_b) of *H at the diverse oxygen sites in "44" structure and "29" structure of CuO_x/Cu(111) models. See Figure 1 panel c and d for detailed labelling.

B. Reaction of H_2 with $ZnO/CuO_x/Cu(111)$ surfaces

B.1 Surface morphology of pristine and H_2 reduced $ZnO/CuO_x/Cu(111)$ surfaces: STM studies

To understand the dynamic morphological changes that could accompany the reduction of an inverse ZnO/CuO_x catalysts[3] by H_2, we performed STM experiments on pristine and H_2-exposed $ZnO/CuO_x/Cu(111)$ systems. Figure 6a shows a wide-scale STM image obtained after depositing zinc at 600 K, under a 5 x 10^{-7} Torr oxygen background onto CuO_x/Cu(111). The morphology reveals that triangular ZnO islands decorate near the step edges of the CuO_x as observed previously by Mahapatra et.al.[30]. These islands are about 150 nm x 80 nm in size and 4 nm in height. Assuming 3.3 Å as the average height of a single-layer of zinc oxide[30], we estimate that the islands consisted

of 8 – 10 layers of zinc oxide. Along with zinc oxide islands, the surface also shows copper oxide terraces as well. These copper oxide terraces are much smaller than the pristine oxide in CuO_x/Cu(111), which could be due to compression caused to accommodate the ZnO islands[32]. The surface that produced the image in Figure 6a had a ZnO coverage of ~ 0.3 ML and exhibited large regions consisting of plain CuO_x/Cu(111) with morphologies similar to those seen in Figure 1[32]. Near the ZnO islands, STM showed some defects in the structure of the copper oxide overlayer, but in general the junction of the ZnO islands and the CuO_x regions was smooth (Figure 6a) as seen in previous studies.[30]

Exposing the ZnO/CuO_x/Cu(111) surface to 50 mTorr H_2 for a cumulative time of 1 hour leads to significant changes in the perimeter of the ZnO islands (Figure 6b). Reduction is quite evident near the ZnO/CuO_x interface; however, some CuO_x regions can be seen further away from the ZnO islands. Nyberg and coworkers predicted the corner sites of ZnO particles as the preferred sites for H_2 dissociation with the central terrace sites being largely inactive[24]. In agreement with their predictions, we speculate that H_2 dissociation at the corner sites might lead to hydrogen spillover at the ZnO – CuO_x interface reducing the CuO_x domains located at the periphery of the ZnO islands. Moreover, the larger concentration of defects in the copper oxide around the ZnO islands could further contribute to enhancing the rate of H_2 dissociation and copper oxide reduction (see above). The dissociated hydrogen could also form a hydroxyl species that could diffuse into the subsurface of ZnO as observed by Mun et. al during AP-XPS measurements of H_2 reduction of ZnO(0001)[26]. The hydroxyl species diffused in the subsurface of ZnO could further react with the hydrogen at the ZnO – CuO_x interface, thereby forming H_2O and causing the reduction of CuO_x located at the perimeter of the ZnO islands.

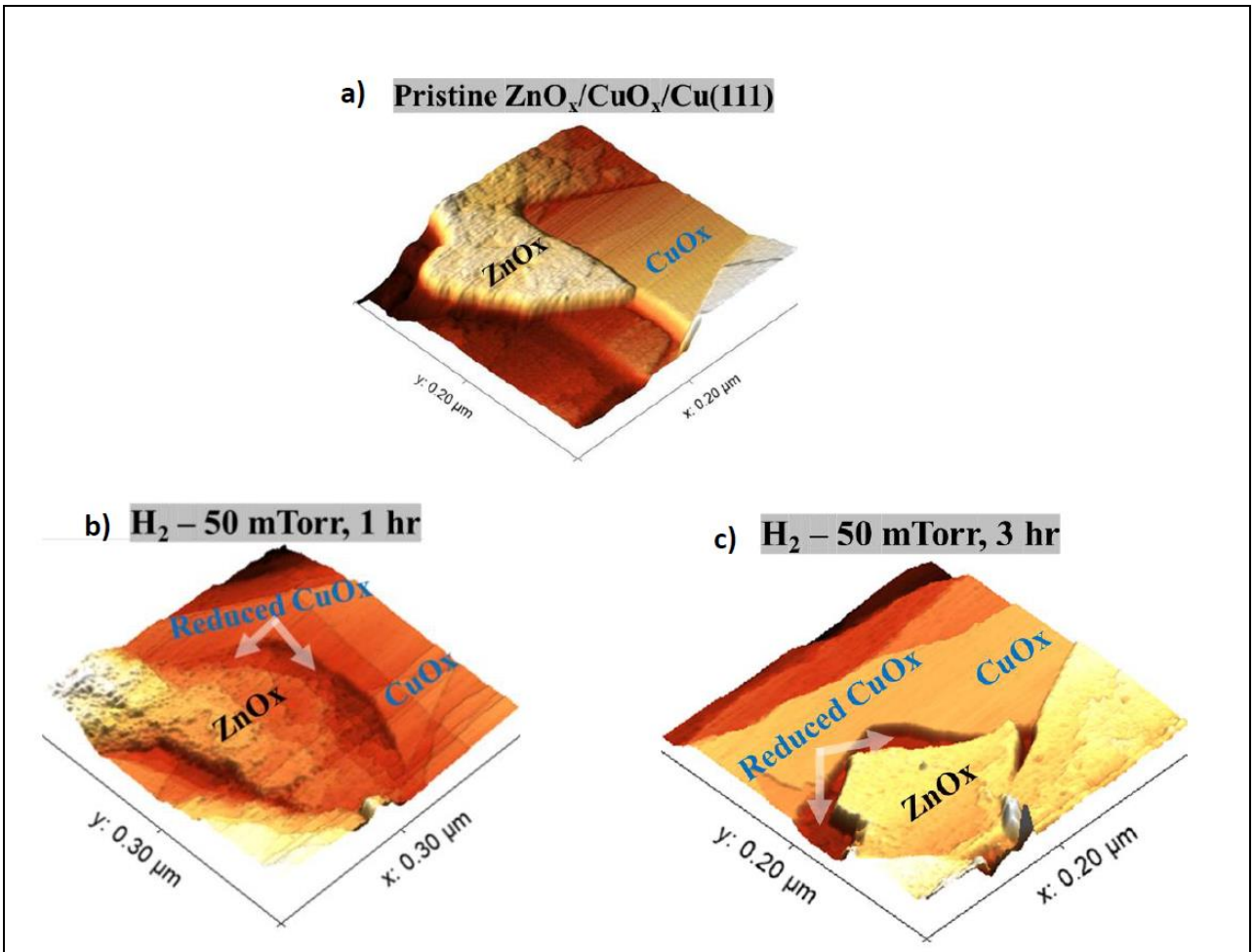

Figure 6: STM images (200 nm x 200 nm) (1500 mV, 1 nA) from a) ZnO_x grown on pristine $CuO_x/Cu(111)$ by vapor depositing Zn in 5 x 10^{-7} Torr O_2 at 600 K and b) after exposing $ZnO_x/CuO_x/Cu(111)$ to 50 mTorr H_2 for 1 hour and c) cumulative 3 hours at 300 K.

A comparison of the images in Figures 2a and 6b shows that the presence of ZnO islands opened reduction channels not seen in plain $CuO_x/Cu(111)$. The induction period was completely absent in areas near the ZnO and was only seen in regions with pure copper oxide. The removal of O from the CuO_x-ZnO interfaces occurred at a rate that was comparable to that seen for the reduction of $CuO_x/Cu(111)$ by CO in Figure 3 and no stable copper oxide structures were observed near the perimeter of the ZnO islands. The bottleneck of dissociating H_2 was not seen on $ZnO_x/CuO_x/Cu(111)$. The results in Figure 6 are consistent with a process where there was fast

dissociation of H_2 on the ZnO islands with a subsequent spillover of H adtoms towards the copper oxide. Near the perimeter of the ZnO islands, the rate for CuO_x reduction was determined by the strength of the bond between the oxygen and copper cations.

B.2 AP-XPS characterization of pristine and H_2 reduced ZnO/CuO_x/Cu(111)

We performed lab-based AP-XPS measurements to gain information on the evolution of the chemical state of O and Zn species during H_2 adsorption on an inverse ZnO/CuO_x/Cu(111) surface. Zinc was vapor deposited in 5 x 10^{-7} Torr O_2 background at 600 K on a pristine CuO_x/Cu(111) substrate to obtain ZnO islands[32]. The surface was then exposed to 50 mTorr of H_2 at 300 K and the spectra were collected as a function of H_2 exposure time. Figure 7 shows Zn 2p and O 1s peaks collected for a pristine ZnO/CuO_x/Cu(111) surface and after 3 hours of H_2 dose (50 mTorr) at 300 K. A close inspection in the Zn 2p peaks (Figure 7a) reveals negligible differences in the pristine and H_2 reduced surfaces. This implies that the oxidation state of Zn was not affected during the H_2 exposure. This point was also verified by taking the Zn LMM Auger that is extremely sensitive to changes in the oxidation state of zinc[58, 59].

In Figure 7b, the O 1s peak at 529.9 eV represents a convolution of the signals for CuO_x (dominant) and ZnO[59]. Since a lab-based AP-XPS instrument was used for this experiment, we could not resolve these different O 1s features. The O 1s peak for ZnO nanoparticles dispersed on Cu(111) appears in the range of 530 - 530.5 eV[59]. Interestingly, upon H_2 exposure, the O 1s features in Figure 7b and S2 upshift by 0.4 eV, which is consistent with a reduction of the surface and a decrease in the CuO/ZnO ratio[59]. Since the Zn 2p and Zn LMM Auger spectra did not change, only the copper oxide component was reduced by hydrogen. Mun and coworkers also investigated H_2 dissociation on ZnO(0001) using AP-XPS[26]. They observed a significant broadening of the O 1s peak and attributed the feature to OH species. In accordance with their findings, we observe ~

22% broadening on the higher binding energy side of the O 1s spectra after H_2 exposure. This broadening of the O 1s peak could be due to the formation of OH species at ~531.4 eV as previously observed in the XPS study of H_2 dissociation on the ZnO(0001) surface suggesting a dissociative adsorption of H_2[26]. As mentioned above, this behavior is also consistent with the reduction of CuO_x, while retaining ZnO domains as seen in the STM (Figure 6b and 6c) and XPS (Figure 7, S2) data.

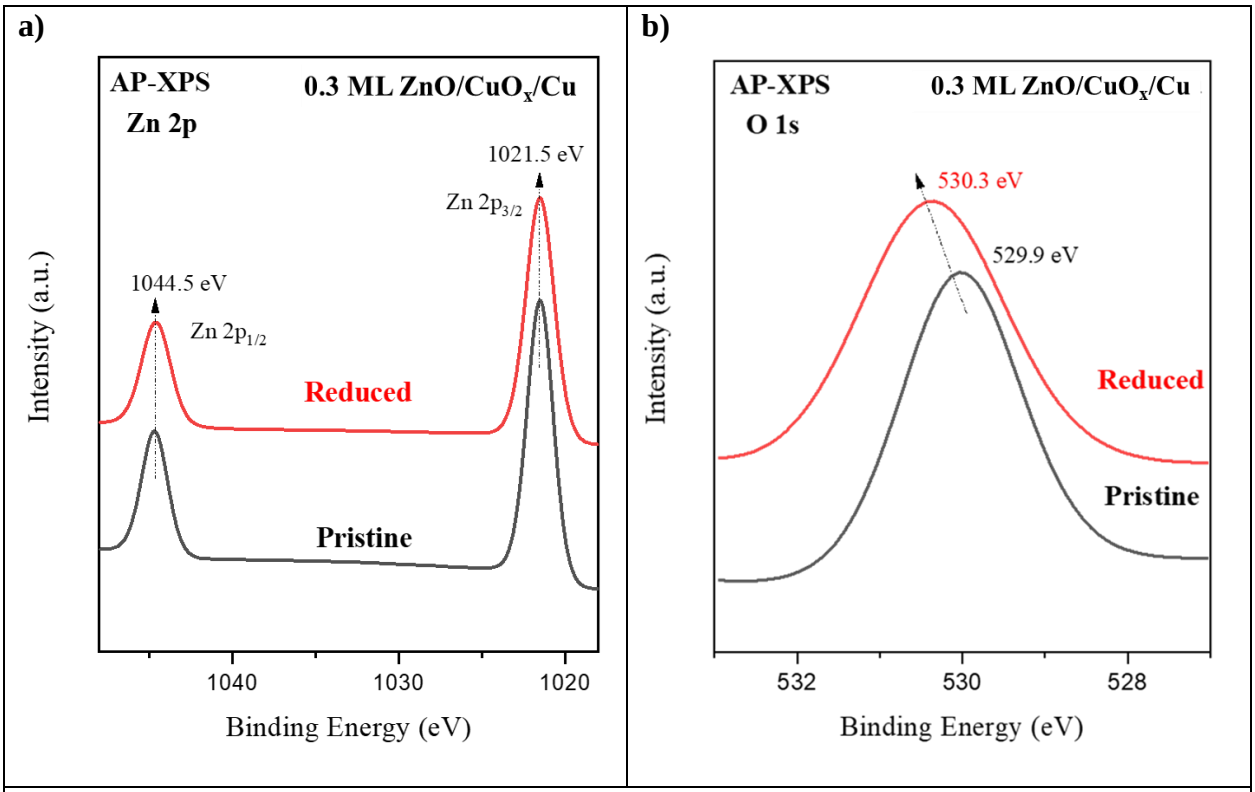

Figure 7: (a) Zn 2p and (b) O 1s spectra from pristine $ZnO_x/CuO_x/Cu(111)$ and after exposing the surface to 50 mTorr of H_2 for 3 hours at 300 K.

B.3 DFT calculations of H_2 binding, dissociation, and diffusion on ZnO/CuO_x*/Cu(111)*

The drastic increase in the rate of surface reduction seen in the STM images of Figure 6 and AP-XPS data of Figure 7 could be explained if one assumes a fast dissociation of H_2 on the

ZnO islands and spillover of H adatoms toward the CuO_x regions. DFT calculations were further performed to understand the effects of depositing ZnO onto CuO_x/Cu(111) model catalysts, where three models (step-rich Zn_3O_3 cluster model, stoichiometric ZnO overlayer model and O-rich ZnO overlayer model) were adopted to describe the step sites, terrace sites and defects sites of ZnO/CuO_x/Cu(111) according to our previous studies (Figure 8) [47, 48]. The ZnO islands seen in

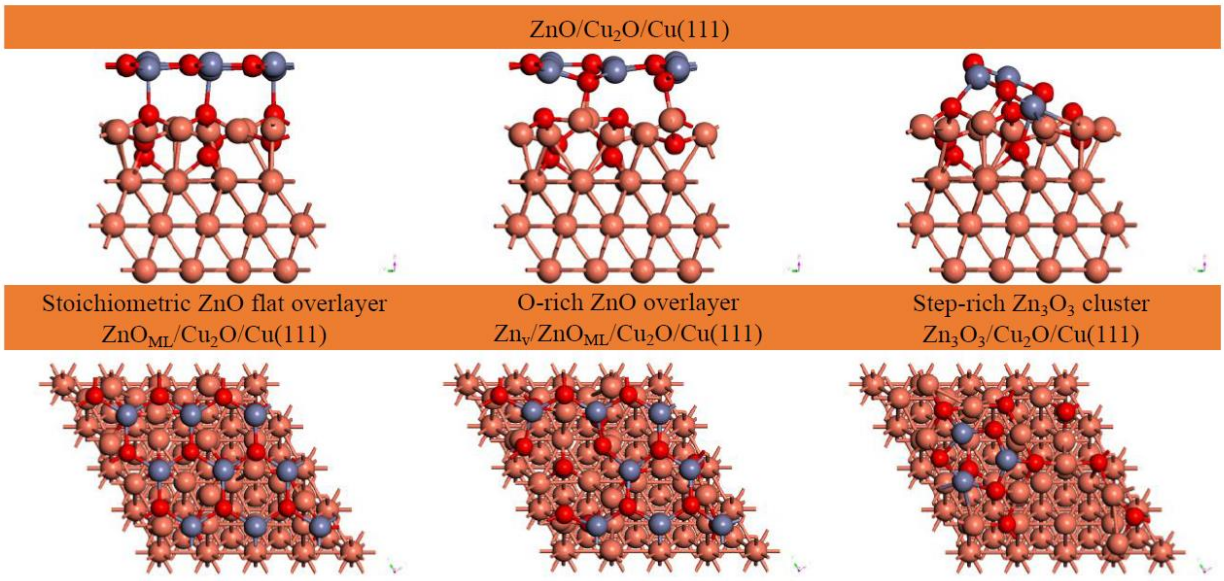

Figure 8. Top and side views of DFT optimized structures for a ZnO flat overlayer, O-rich ZnO overlayer, and a Zn_3O_3 cluster model. Color code: violet is Zn; red is O; brown is Cu.

the STM images have rough surfaces with diverse sites[30] that were modeled using the structures seen in Figure 8. These structures represent well the chemical properties of ZnO/CuO_x/Cu(111).[47,48] They are different from a typical termination of bulk ZnO[24,26] or from supported bilayer films of ZnO on Cu(111).[25] One of them has Zn vacancies in a ZnO overlayer (O-rich ZnO) and the chemistry of another is determined by the presence of partially coordinated

Zn and O sites (Zn_3O_3 cluster). The structures in Figure 8 represent different types of adsorption sites that a H_2 molecule will find when adsorbing on the ZnO islands depicted in Figure 6a. In principle the molecule can interact with Zn or O cations.

As seen for CuO_x/Cu(111), the oxygen site at the ZnO-CuO_x interface was preferred by dissociated *H fragments. Wherein, the low-coordinated oxygen site in O-rich ZnO overlayer model showed a strong binding to *H species (Figure 9a, ΔE_b: -2.07 eV), followed by the step-rich Zn_3O_3 cluster model (ΔE_b: -1.20 eV) and the stoichiometric ZnO overlayer model (ΔE_b: -0.96 eV) in a decreasing sequence. A similar sequence was observed previously for CH_4 dissociation [47], and reflected the occupancy of oxygen 2p states at each type of sites[47]. Nevertheless, all the three types of sites in the ZnO/CuO_x/Cu(111) models showed higher binding to *H species than that of the CuO_x/Cu(111) model (Figure 5). As a result, a promoted H_2 dissociation by depositing ZnO on a CuO_x/Cu(111) substrate is expected (Figure 9b). Indeed, the H_2 dissociation on the step-rich Zn_3O_3 cluster model (reaction energy, ΔE: -2.00 eV), for instance, is thermodynamically more favorable than that of CuO_x/Cu(111) (ΔE: -0.99 eV).

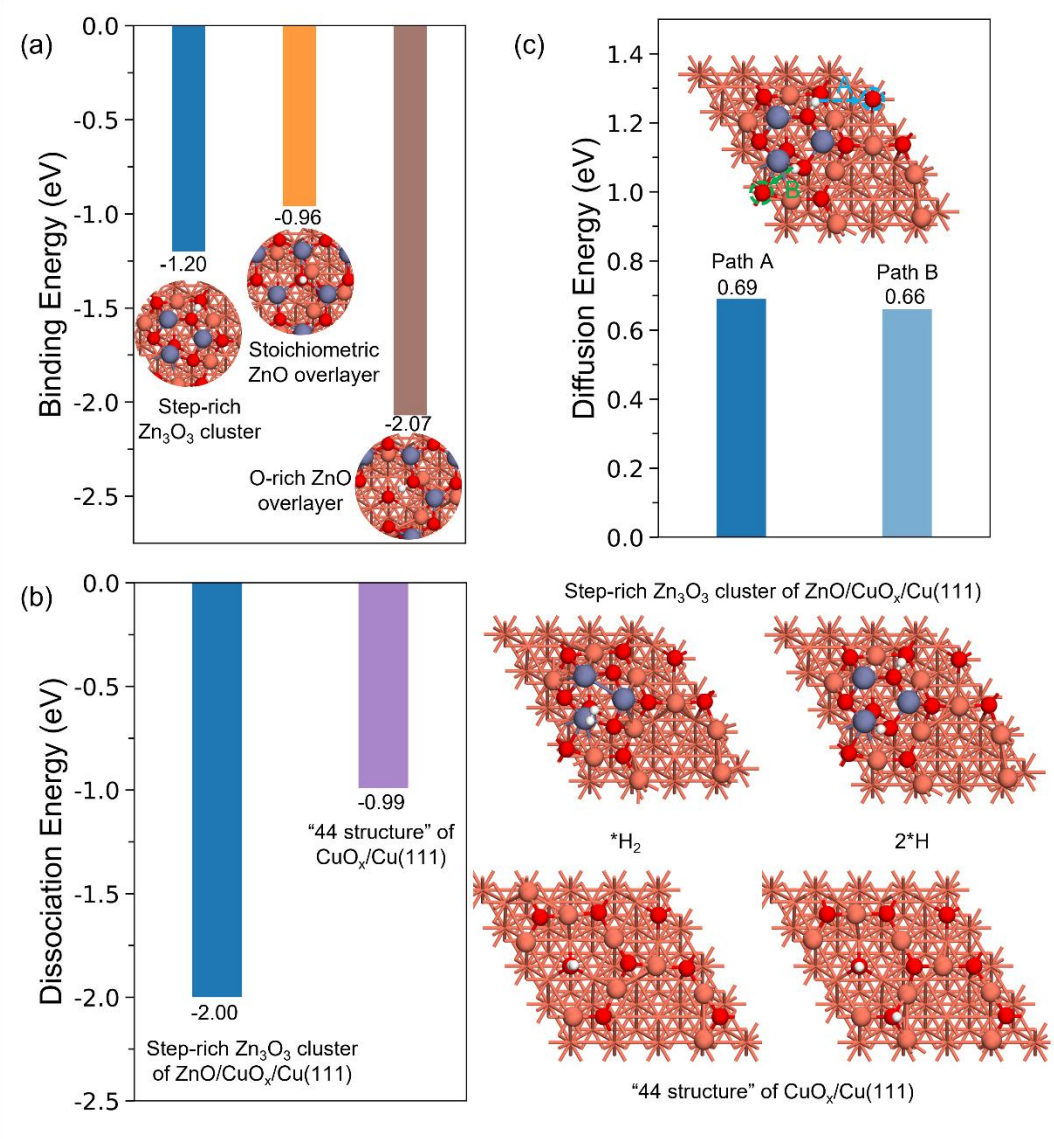

Figure 9: (a) DFT-calculated binding energies (ΔE_b) of *H species on the ZnO/CuO_x/Cu(111) model catalysts, including step-rich Zn_3O_3 cluster model, stoichiometric ZnO overlayer model, and O-rich ZnO overlayer model. Inset: DFT-optimized structures for *H binding on three models of ZnO/CuO_x/Cu(111) model catalysts. (b) DFT-calculated H_2 adsorption and dissociation on step-rich Zn_3O_3 cluster model of ZnO/CuO_x/Cu(111) and "44 structure" of CuO_x/Cu(111) model catalysts and their corresponding DFT-optimized structures. (c) Schematics for DFT-calculated

*H diffusion paths on the step-rich Zn_3O_3 cluster model of ZnO/CuO_x/Cu(111) model catalyst. Violet: Zn; Brown: Cu; Red: O; White: H.

In addition, the dissociated *H prefers to spillover from ZnO to CuO_x at the perimeter region. Specifically, the diffusion of *H from the most stable oxygen site at the step-rich Zn_3O_3 cluster to the O_{NL} (Figure 9c, Path A) and O_L sites (Figure 9c, Path B) of CuO_x at the boundary requires to overcome reaction energies of 0.69 eV and 0.66 eV, respectively. By comparison, the removal of interacted oxygen from supported ZnO was found to be much more difficult (oxygen vacancy formation energy: $E_f(Ov)$ = 2.37 eV) according to our previous study.[47] Under the temperature range considered experimentally, the mild endothermicity for hydrogen spillover is likely to be overcome, being able to facilitate the reduction of Cu_2O layer as observed experimentally as compared to the case of CuO_x/Cu(111) (Figure 6). In a dynamic process, H adatoms move from ZnO to CuO_x, opening sites on which additional H_2 molecules can dissociate.

Discussion

Our AP-XPS and AP-STM results for CuO_x/Cu(111) agree well with previous studies, [14-16] showing kinetically limited H_2 dissociation (Figures 2 and 4) and a long induction time that plays a central role in an autocatalytic process (Figure 2). During this induction time, there is only a small amount of OH groups on the surface and, according to the results of AP-XPS studies and DFT calculations, the H_2 molecules mainly react with non-lattice oxygen atoms to form H_2O molecules. For both 44- and 29-structures of CuO_x/Cu(111), the non-lattice oxygen sites are more active to hydrogen dissociation than the lattice oxygen sites as shown by DFT results and are likely more easily to be removed by hydrogenation as observed by AP-XPS (Figure 4). As a result, the

stoichiometric CuO_x framework on Cu(111) can be well maintained to hinder the reduction on exposure to hydrogen, while proceeding of the reaction strongly depends on the under-coordinated and defect sites as observed by AP-STM (Figure 2). Thus, a large induction period (> 1 hour) played a central role in an autocatalytic process (Figure 2). This increases the concentration of defects and should be the prelude to the generation of the reaction fronts seen in previous studies of STM and TEM[11-14].

The addition of ZnO to CuO_x/Cu(111) drastically changed the chemical behavior of the system and opened new channels for the reduction process. The presence of ZnO islands substantially accelerated the rate of H_2 activation and the reduction of the copper oxide located around these islands as observed by our AP-STM and AP-XPS results (Figures 6 and 7) Wherein, a large fraction (~ 20 %) of the surface oxygen at the ZnO-CuO_x interface was removed in the first hour of H_2 exposure (Figures S2 and S3). According to the DFT calculations (Figure 8a), the deposited ZnO can provide active oxygen sites to strengthen hydrogen binding and facilitate H_2 activation on CuO_x/Cu(111). The stability of ZnO prevented its reduction and enabled facile spillover of dissociated *H species to CuO_x regions (Figure 8b), accelerating the reduction of the copper oxide component as seen in Figure 6. It has been proposed that additional reduction of Cu/ZnO by H_2 could create an active CuZn alloy phase for the synthesis of methanol through CO_2 hydrogenation[2, 3, 5, 60]. Our studies showed that on exposure to ambient pressures, the interaction of H_2 with ZnO/CuO_x/Cu(111) only led to reduction of the copper oxide with the ZnO remaining intact. Given that, the Cu/ZnO phase is more likely to form the active sites under CO_2 hydrogenation conditions.

Furthermore, the presence of defects near the CuO_x-ZnO interface should facilitate the reduction of copper oxide domains. Defective copper oxide has also been seen in STM studies for

the deposition of nanoparticles of CeO_2, ZrO_2 and SnO_2 on CuO_x/Cu(111)[18-21,61]. Thus, independently of the ability of the added oxide overlayer to dissociate H_2, the presence of surface defects around the nanoparticles of CeO_2, ZrO_2 and SnO_2 should enhance the reduction rate, but the drastic morphological changes seen in Figure 6b,c for ZnO/CuO_x/Cu(111) are more consistent with H spillover from ZnO. Furthermore, nanoparticles of CeO_2, ZrO_2 and SnO_2 are all more reactive towards H_2 dissociation than copper oxide[18, 20, 21, 62], thus opening the possibility of hydrogen spillover from the oxide overlayer onto the oxide substrate. This key property of the CuO_x-MO interfaces (MO= ZnO, CeO_2, ZrO_2 and SnO_2) must be taken into consideration when optimizing their performance for the hydrogenation of CO_2. Our results show that the H adatoms generated on top of the ZnO structures are very mobile and can be used for hydrogenation processes on the copper. Indeed, in previous studies we found a more active surface chemistry for CO_2/H_2 on ZnO/Cu(111) than on Cu(111).[30.31] On ZnO/Cu(111), formate (H + CO_2 → HCOO) was generated as an active intermediate for methanol production.[30,31,59]

The dissociation of H_2 on cu-based catalysts is a key step in the conversion of CO_2 to methanol.[2-5,8] The CO_2 does not bind well to copper surfaces and H adatoms do facilitate the binding of the molecule.[59,63] Furthermore, the surface chemistry associated with a CO_2 → CH_3OH transformation is usually facilitated by H-rich surfaces.[2,20,23,59,63] Taking this into consideration, we can conclude that the addition of ZnO to copper is a very important step for the catalytic conversion of CO_2. DFT results show exothermic processes for the dissociation of H_2 on nanoparticles (ΔE: -2.00 eV, Figure 9) and bilayer films (ΔE: -1.5 eV)[25] of ZnO supported on Cu(111). The existence of corner and edge atoms in the supported ZnO facilitates H-H bond cleavage (Figure 9) and the results of STM (Figure 6) and XPS (Figure 7) show that H migration to the copper component is not a difficult process even at room temperature. When dealing with

the CO_2 → CH_3OH reaction, an inverse ZnO/Cu configuration has chemical properties not seen for bulk surfaces of pure copper or zinc oxide,[24-26] and its ability to activate H_2 and release H adatoms is a very important characteristic.

Summary

The reduction of pristine CuO_x/Cu(111) and ZnO/CuO_x/Cu(111) by H_2 was investigated using AP-STM, AP-XPS and DFT calculations. The morphological changes and reaction rates seen for the reduction of CuO_x/Cu(111) and ZnO/CuOx/Cu(111) are very different. On CuO_x/Cu(111), a large induction period (associated with the creation of surface defects) played a central role in an autocatalytic process that involved the dissociation of H_2 and the formation of water. During this induction period, the amounts of OH and H_2O present on the oxide surface are minimal (< 0.05 ML). At the initial stages, the "29" and "44" structures of copper oxide were reduced by removal of chemisorbed non-lattice oxygen, and sequentially lattice oxygen due to their difference in *H binding capacity, which eventually was transformed into ordered oxygen-deficient "5-7 hex" and honeycomb-like structures before forming domains of chemisorbed oxygen species and metallic copper. During the reduction process, the oxygen from the surface layers reacted with H_2 to produce water, and the vacancies generated during the reduction process were refilled by the diffusion of oxygen from the bulk to the surface layers.

Zinc oxide islands grew as triangular shaped islands on the terraces of CuO_x/Cu(111). The mechanisms for the reduction of CuO_x/Cu(111) and ZnO/CuO_x/Cu(111) are very different. H_2 readily dissociated on ZnO islands, and the migration of H atoms resulted in the fast reduction of copper oxide regions located in the perimeter of the zinc oxide structures. These results further

demonstrate that H_2 dissociation is kinetically limited on pristine CuO_x/Cu(111) due to a lack of defects and coordinatively unsaturated sites. The STM and AP-XPS results point to two clear regions during the reduction of ZnO/CuO_x/Cu(111). DFT calculations further confirmed the significantly more favorable binding and dissociation of H_2 at the ZnO-CuO_x interfaces and the facile diffusion of surface *H species from ZnO to CuO_x regions. This key property of ZnO - CuO_x interfaces must be taken into consideration when optimizing their performance for the hydrogenation of CO_2.

Acknowledgments

Most of this research was conducted at the Chemistry Division of Brookhaven National Laboratory and supported by the Office of Basic Energy Sciences of the US Department of Energy (DOE) under contract No DE-SC0012704 through BNL-FWP CO-040. Part of the photoemission and theoretical studies were supported by the US-DOE under contract No DE-SC0012704 through BNL-FWP CO-060. This research used resources of beamline 23-ID-2 (IOS) of the National Synchrotron Light Source II, a U.S. Department of Energy (DOE) Office of Science User Facility operated for the DOE Office of Science by Brookhaven National Laboratory under contract No. DE-SC0012704. The DFT calculations were performed using computational resources at the Center for Functional Nanomaterials (CFN), which is a U.S. Department of Energy Office of Science User Facility, at Brookhaven National Laboratory, and at the National Energy Research Scientific Computing Center (NERSC), a U.S. Department of Energy Office of Science User Facility located at Lawrence Berkeley National Laboratory, operated under Contract No. DE-AC02-05CH11231.

References

1. Inventory of U.S. Greenhouse Gas Emissions and Sinks. *https://www.epa.gov/ghgemissions/inventory-us-greenhouse-gas-emissions-and-sinks* **Accessed 2023**.
2. Divins, N. J.; Kordus, D.; Timoshenko, J.; Sinev, I.; Zegkinoglou, I.; Bergmann, A.; Chee, S. W.; Widrinna, S.; Karslıoğlu, O.; Mistry, H.; Lopez Luna, M.; Zhong, J. Q.; Hoffman, A. S.; Boubnov, A.; Boscoboinik, J. A.; Heggen, M.; Dunin-Borkowski, R. E.; Bare, S. R.; Cuenya, B. R., Operando high-pressure investigation of size-controlled CuZn catalysts for the methanol synthesis reaction. *Nat. Commun.* **2021,** *12* (1), 1435.
3. Lunkenbein, T.; Schumann, J.; Behrens, M.; Schlögl, R.; Willinger, M. G., Formation of a ZnO Overlayer in Industrial Cu/ZnO/Al_2O_3 Catalysts Induced by Strong Metal–Support Interactions. *Angew. Chem. Int. Ed.* **2015,** *54* (15), 4544-4548.
4. Behrens, M.; Studt, F.; Kasatkin, I.; Kühl, S.; Hävecker, M.; Abild-Pedersen, F.; Zander, S.; Girgsdies, F.; Kurr, P.; Kniep, B.-L.; Tovar, M.; Fischer, R. W.; Nørskov, J. K.; Schlögl, R., The Active Site of Methanol Synthesis over Cu/ZnO/Al_2O_3 Industrial Catalysts. *Science* **2012,** *336* (6083), 893-897.
5. Kattel, S.; Ramírez, P. J.; Chen, J. G.; Rodriguez, J. A.; Liu, P., Active sites for CO_2 hydrogenation to methanol on Cu/ZnO catalysts. *Science* **2017,** *355* (6331), 1296-1299.
6. Studt, F.; Behrens, M.; Kunkes, E. L.; Thomas, N.; Zander, S.; Tarasov, A.; Schumann, J.; Frei, E.; Varley, J. B.; Abild-Pedersen, F.; Nørskov, J. K.; Schlögl, R., The Mechanism of CO and CO_2 Hydrogenation to Methanol over Cu-Based Catalysts. *ChemCatChem* **2015,** *7* (7), 1105-1111.
7. Li, W.; Cui, X.; Junge, K.; Surkus, A.-E.; Kreyenschulte, C.; Bartling, S.; Beller, M., General and Chemoselective Copper Oxide Catalysts for Hydrogenation Reactions. *ACS Catal.* **2019,** *9* (5), 4302-4307.
8. Zhang, Z.; Chen, X.; Kang, J.; Yu, Z.; Tian, J.; Gong, Z.; Jia, A.; You, R.; Qian, K.; He, S.; Teng, B.; Cui, Y.; Wang, Y.; Zhang, W.; Huang, W., The active sites of Cu–ZnO catalysts for water gas shift and CO hydrogenation reactions. *Nat. Commun.* **2021,** *12* (1), 4331.
9. Yang, F.; Graciani, J.; Evans, J.; Liu, P.; Hrbek, J.; Sanz, J. F.; Rodriguez, J. A., CO Oxidation on Inverse CeOx/Cu(111) Catalysts: High Catalytic Activity and Ceria-Promoted Dissociation of O_2. *J. Am. Chem. Soc.* **2011,** *133* (10), 3444-3451.
10. Zhang, Z.; Wang, S.-S.; Song, R.; Cao, T.; Luo, L.; Chen, X.; Gao, Y.; Lu, J.; Li, W.-X.; Huang, W., The most active Cu facet for low-temperature water gas shift reaction. *Nat. Commun.* **2017,** *8* (1), 488.
11. Kim, J. Y.; Rodriguez, J. A.; Hanson, J. C.; Frenkel, A. I.; Lee, P. L., Reduction of CuO and Cu2O with H2: H Embedding and Kinetic Effects in the Formation of Suboxides. *J. Am. Chem. Soc.* **2003,** *125* (35), 10684-10692.
12. Günter, M. M.; Ressler, T.; Jentoft, R. E.; Bems, B., Redox Behavior of Copper Oxide/Zinc Oxide Catalysts in the Steam Reforming of Methanol Studied by in Situ X-Ray Diffraction and Absorption Spectroscopy. *J. Catal.* **2001,** *203* (1), 133-149.
13. Unutulmazsoy, Y.; Cancellieri, C.; Lin, L.; Jeurgens, L. P. H., Reduction of thermally grown single-phase CuO and Cu_2O thin films by in-situ time-resolved XRD. *Appl. Surf. Sci.* **2022,** *588*, 152896.
14. Xu, F. In situ Ambient Pressure Studies of Dynamic Surface Transformations on Cu-based Model Catalysts. The Graduate School, Stony Brook University: Stony Brook, NY., Stony Brook, NY, 2016.
15. Sun, X.; Wu, D.; Zhu, W.; Chen, X.; Sharma, R.; Yang, J. C.; Zhou, G., Atomic Origin of the Autocatalytic Reduction of Monoclinic CuO in a Hydrogen Atmosphere. *J. Phys. Chem. Lett.* **2021,** *12* (39), 9547-9556.
16. Sun, X.; Wu, D.; Zou, L.; House, S. D.; Chen, X.; Li, M.; Zakharov, D. N.; Yang, J. C.; Zhou, G., Dislocation-induced stop-and-go kinetics of interfacial transformations. *Nature* **2022,** *607* (7920), 708-713.

17. Hao, G.; Zhang, R.; Li, J.; Wang, B.; Zhao, Q., Insight into the effect of surface structure on H_2 adsorption and activation over different CuO(111) surfaces: A first-principle study. *Comput. Mater. Sci.* **2016,** *122*, 191-200.
18. Huang, E.; Rui, N.; Rosales, R.; Kang, J.; Nemšák, S.; Senanayake, S. D.; Rodriguez, J. A.; Liu, P., Highly selective methane to methanol conversion on inverse $SnO_2/Cu_2O/Cu(111)$ catalysts: Unique properties of SnO_2 nanostructures and the inhibition of the direct oxidative combustion of methane. *ACS Catal.* **2022,** *12* (18), 11253-11262.
19. Kang, J.; Rui, N.; Huang, E.; Tian, Y.; Mahapatra, M.; Rosales, R.; Orozco, I.; Shi, R.; Senanayake, S. D.; Liu, P.; Rodriguez, J. A., Surface characterization and methane activation on $SnO_x/Cu_2O/Cu(111)$ inverse oxide/metal catalysts. *Phys. Chem. Chem. Phys.* **2021,** *23* (32), 17186-17196.
20. Graciani, J.; Mudiyanselage, K.; Xu, F.; Baber, A. E.; Evans, J.; Senanayake, S. D.; Stacchiola, D. J.; Liu, P.; Hrbek, J.; Sanz, J. F.; Rodriguez, J. A., Highly active copper-ceria and copper-ceria-titania catalysts for methanol synthesis from CO_2. *Science* **2014,** *345* (6196), 546-550.
21. Rui, N.; Shi, R.; Gutiérrez, R. A.; Rosales, R.; Kang, J.; Mahapatra, M.; Ramírez, P. J.; Senanayake, S. D.; Rodriguez, J. A., CO2 Hydrogenation on $ZrO_2/Cu(111)$ Surfaces: Production of Methane and Methanol. *Ind. Eng. Chem. Res.* **2021,** *60* (51), 18900-18906.
22. Wu, C.; Lin, L.; Liu, J.; Zhang, J.; Zhang, F.; Zhou, T.; Rui, N.; Yao, S.; Deng, Y.; Yang, F.; Xu, W.; Luo, J.; Zhao, Y.; Yan, B.; Wen, X.-D.; Rodriguez, J. A.; Ma, D., Inverse ZrO_2/Cu as a highly efficient methanol synthesis catalyst from CO_2 hydrogenation. *Nat. Commun.* **2020,** *11* (1), 5767.
23. Rui, N.; Wang, X.; Deng, K.; Moncada, J.; Rosales, R.; Zhang, F.; Xu, W.; Waluyo, I.; Hunt, A.; Stavitski, E.; Senanayake, S. D.; Liu, P.; Rodriguez, J. A., Atomic Structural Origin of the High Methanol Selectivity over In_2O_3–Metal Interfaces: Metal–Support Interactions and the Formation of a InOx Overlayer in Ru/In2O3 Catalysts during CO_2 Hydrogenation. *ACS Catal.* **2023**, 3187-3200.
24. Nyberg, M.; Nygren, M. A.; Pettersson, L. G. M.; Gay, D. H.; Rohl, A. L., Hydrogen Dissociation on Reconstructed ZnO Surfaces. *J. Phys. Chem.* **1996,** *100* (21), 9054-9063.
25. Thang, H. V.; Pacchioni, G., H_2 Adsorption on Wurtzite ZnO and on ZnO/M(111) (M=Cu, Ag and Au) Bilayer Films. *ChemNanoMat* **2019,** *5* (7), 932-939.
26. Mun, B. S.; Liu, Z.; Motin, M. A.; Roy, P. C.; Kim, C. M., In situ observation of H_2 dissociation on the ZnO (0001) surface under high pressure of hydrogen using ambient-pressure XPS. *Int. J. Hydrogen Energy* **2018,** *43* (18), 8655-8661.
27. Yang, F.; Choi, Y.; Liu, P.; Hrbek, J.; Rodriguez, J. A., Autocatalytic Reduction of a $Cu_2O/Cu(111)$ Surface by CO: STM, XPS, and DFT Studies. *J. Phys. Chem. C* **2010,** *114* (40), 17042-17050.
28. Jensen, F.; Besenbacher, F.; Stensgaard, I., Two new oxygen induced reconstructions on Cu(111). *Surf. Sci.* **1992,** *269-270*, 400-404.
29. Matsumoto, T.; Bennett, R. A.; Stone, P.; Yamada, T.; Domen, K.; Bowker, M., Scanning tunneling microscopy studies of oxygen adsorption on Cu(111). *Surf. Sci.* **2001,** *471* (1), 225-245.
30. Mahapatra, M.; Kang, J.; Ramírez, P. J.; Hamlyn, R.; Rui, N.; Liu, Z.; Orozco, I.; Senanayake, S. D.; Rodriguez, J. A., Growth, Structure, and Catalytic Properties of ZnO_x Grown on $CuO_x/Cu(111)$ Surfaces. *J. Phys. Chem. C* **2018,** *122* (46), 26554-26562.
31. Palomino, R. M.; Hamlyn, R.; Liu, Z.; Grinter, D. C.; Waluyo, I.; Rodriguez, J. A.; Senanayake, S. D., Interfaces in heterogeneous catalytic reactions: Ambient pressure XPS as a tool to unravel surface chemistry. *J. Electron. Spectrosc. Relat. Phenom.* **2017,** *221*, 28-43.
32. Waluyo, I.; Hunt, A., Ambient Pressure X-Ray Photoelectron Spectroscopy at the IOS (23-ID-2) Beamline at the National Synchrotron Light Source II. *Synchrotron Radiat. News* **2022,** *35* (3), 31-38.
33. Palomino, R. M.; Stavitski, E.; Waluyo, I.; Chen-Wiegart, Y.-c. K.; Abeykoon, M.; Sadowski, J. T.; Rodriguez, J. A.; Frenkel, A. I.; Senanayake, S. D., New In-Situ and Operando Facilities for Catalysis Science at NSLS-II: The Deployment of Real-Time, Chemical, and Structure-Sensitive X-ray Probes. *Synchrotron Radiat. News* **2017,** *30* (2), 30-37.

34. Xu, F.; Mudiyanselage, K.; Baber, A. E.; Soldemo, M.; Weissenrieder, J.; White, M. G.; Stacchiola, D. J., Redox-Mediated Reconstruction of Copper during Carbon Monoxide Oxidation. *J. Phys. Chem. C* **2014,** *118* (29), 15902-15909.
35. Yang, F.; Choi, Y.; Liu, P.; Stacchiola, D.; Hrbek, J.; Rodriguez, J. A., Identification of 5–7 Defects in a Copper Oxide Surface. *J. Am. Chem. Soc.* **2011,** *133* (30), 11474-11477.
36. Kohn, W.; Sham, L. J., Self-consistent equations including exchange and correlation effects. *Phys. Rev.* **1965,** *140* (4A), A1133-A1138.
37. Kresse, G.; Furthmuller, J., Efficient iterative schemes for ab initio total-energy calculations using a plane-wave basis set. *Phys. Rev. B* **1996,** *54* (16), 11169-11186.
38. Blochl, P. E., Projector augmented-wave method. *Phys. Rev. B* **1994,** *50* (24), 17953-17979.
39. Perdew, J. P.; Burke, K.; Ernzerhof, M., Generalized gradient approximation made simple. *Phys. Rev. Lett.* **1996,** *77* (18), 3865-3868.
40. Monkhorst, H. J.; Pack, J. D., Special points for Brillouin-zone integrations. *Phys. Rev. B* **1976,** *13* (12), 5188-5192.
41. Anisimov, V. I.; Zaanen, J.; Andersen, O. K., Band theory and Mott insulators: Hubbard U instead of Stoner I. *Phys. Rev. B* **1991,** *44* (3), 943-954.
42. An, W.; Baber, A. E.; Xu, F.; Soldemo, M.; Weissenrieder, J.; Stacchiola, D.; Liu, P., Mechanistic Study of CO Titration on CuxO/Cu(1 1 1) (x⩽2) Surfaces. *ChemCatChem* **2014,** *6* (8), 2364-2372.
43. An, W.; Xu, F.; Stacchiola, D.; Liu, P., Potassium-Induced Effect on the Structure and Chemical Activity of the Cu_xO/Cu(111) (x <= 2) Surface: A Combined Scanning Tunneling Microscopy and Density Functional Theory Study. *Chemcatchem* **2015,** *7* (23), 3865-3872.
44. Orozco, I.; Huang, E.; Mahapatra, M.; Shi, R.; Kang, J.; Nemšák, S.; Senanayake, S. D.; Liu, P.; Rodriguez, J. A., In situ studies of methanol decomposition over Cu(111) and Cu_2O/Cu(111): Effects of reactant pressure, surface morphology, and hot spots of active sites. *J. Phys. Chem. C* **2020,** *125* (1), 558-571.
45. Therrien, A. J.; Zhang, R.; Lucci, F. R.; Marcinkowski, M. D.; Hensley, A.; McEwen, J.-S.; Sykes, E. C. H., Structurally Accurate Model for the "29"-Structure of Cu_xO/Cu(111): A DFT and STM Study. *J. Phys. Chem. C* **2016,** *120* (20), 10879-10886.
46. Hensley, A. J. R.; Therrien, A. J.; Zhang, R.; Marcinkowski, M. D.; Lucci, F. R.; Sykes, E. C. H.; McEwen, J.-S., CO Adsorption on the "29" Cu_xO/Cu(111) Surface: An Integrated DFT, STM, and TPD Study. *J. Phys. Chem. C* **2016,** *120* (44), 25387-25394.
47. Huang, E.; Orozco, I.; Ramirez, P. J.; Liu, Z.; Zhang, F.; Mahapatra, M.; Nemsak, S.; Senanayake, S. D.; Rodriguez, J. A.; Liu, P., Selective methane oxidation to methanol on ZnO/Cu_2O/Cu(111) catalysts: Multiple site-dependent behaviors. *J. Am. Chem. Soc.* **2021,** *143* (45), 19018-19032.
48. Orozco, I.; Huang, E.; Mahapatra, M.; Kang, J.; Shi, R.; Nemšák, S.; Tong, X.; Senanayake, S. D.; Liu, P.; Rodríguez, J. A., Understanding methanol synthesis on inverse ZnO/CuO_x/Cu catalysts: Stability of CH3O species and dynamic nature of the surface. *J. Phys. Chem. C* **2021,** *125* (12), 6673-6683.
49. Lu, Q.; Hutchings, G. S.; Yu, W.; Zhou, Y.; Forest, R. V.; Tao, R.; Rosen, J.; Yonemoto, B. T.; Cao, Z.; Zheng, H., Highly porous non-precious bimetallic electrocatalysts for efficient hydrogen evolution. *Nat. Commun.* **2015,** *6* (1), 1-8.
50. Besenbacher, F.; Nørskov, J. K., Oxygen chemisorption on metal surfaces: General trends for Cu, Ni and Ag. *Prog. Surf. Sci.* **1993,** *44* (1), 5-66.
51. Jensen, F.; Besenbacher, F.; Lægsgaard, E.; Stensgaard, I., Oxidation of Cu(111): two new oxygen induced reconstructions. *Surf. Sci.* **1991,** *259* (3), L774-L780.
52. Lee, Y.-J.; Ly, T. T.; Lee, T.; Palotás, K.; Jeong, S. Y.; Kim, J.; Soon, A., Completing the picture of initial oxidation on copper. *Appl. Surf. Sci.* **2021,** *562*, 150148.

53. Xu, F.; An, W.; Baber, A. E.; Grinter, D. C.; Senanayake, S. D.; White, M. G.; Liu, P.; Stacchiola, D. J., Enhanced Oxide Reduction by Hydrogen at Cuprous Oxide–Copper Interfaces near Ascending Step Edges. *J. Phys. Chem. C* **2022**.
54. Baber, A. E.; Xu, F.; Dvorak, F.; Mudiyanselage, K.; Soldemo, M.; Weissenrieder, J.; Senanayake, S. D.; Sadowski, J. T.; Rodriguez, J. A.; Matolín, V.; White, M. G.; Stacchiola, D. J., In Situ Imaging of Cu_2O under Reducing Conditions: Formation of Metallic Fronts by Mass Transfer. *J. Am. Chem. Soc.* **2013,** *135* (45), 16781-16784.
55. Wiame, F.; Maurice, V.; Marcus, P., Initial stages of oxidation of Cu(111). *Surf. Sci.* **2007,** *601* (5), 1193-1204.
56. Kahk, J. M.; Lischner, J., Core electron binding energies of adsorbates on Cu(111) from first-principles calculations. *Phys. Chem. Chem. Phys.* **2018,** *20* (48), 30403-30411.
57. Schilling, A. C.; Groden, K.; Simonovis, J. P.; Hunt, A.; Hannagan, R. T.; Çınar, V.; McEwen, J.-S.; Sykes, E. C. H.; Waluyo, I., Accelerated Cu_2O Reduction by Single Pt Atoms at the Metal-Oxide Interface. *ACS Catal.* **2020,** *10* (7), 4215-4226.
58. Schön, G., Auger and direct electron spectra in X-ray photoelectron studies of zinc, zinc oxide, gallium and gallium oxide. *J. Electron. Spectrosc. Relat. Phenom.* **1973,** *2* (1), 75-86.
59. Palomino, R. M.; Ramírez, P. J.; Liu, Z.; Hamlyn, R.; Waluyo, I.; Mahapatra, M.; Orozco, I.; Hunt, A.; Simonovis, J. P.; Senanayake, S. D.; Rodriguez, J. A., Hydrogenation of CO_2 on ZnO/Cu(100) and ZnO/Cu(111) Catalysts: Role of Copper Structure and Metal–Oxide Interface in Methanol Synthesis. *J. Phys. Chem. B* **2018,** *122* (2), 794-800.
60. Saedy, S.; Newton, M. A.; Zabilskiy, M.; Lee, J. H.; Krumeich, F.; Ranocchiari, M.; van Bokhoven, J. A., Copper–zinc oxide interface as a methanol-selective structure in Cu–ZnO catalyst during catalytic hydrogenation of carbon dioxide to methanol. *Catal. Sci. Technol.* **2022,** *12* (8), 2703-2716.
61. Shi, R.; Mahapatra, M.; Kang, J.; Orozco, I.; Senanayake, S. D.; Rodriguez, J. A., Preparation and Structural Characterization of ZrO_2/CuOx/Cu(111) Inverse Model Catalysts. *J. Phys. Chem. C* **2020,** *124* (19), 10502-10508.
62. Rui, N.; Huang, E.; Kim, J.; Mehar, V.; Shi, R.; Rosales, R.; Tian, Y.; Hunt, A.; Waluyo, I.; Senanayake, S. D.; Liu, P.; Rodriguez, J. A., CO_2 hydrogenation to methanol over inverse ZrO_2/Cu(111) catalysts: The fate of methoxy under dry and wet conditions. *J. Phys. Chem. C* **2022,** *126* (34), 14479-14486.
63. Yang, Y; Evans, J.; Rodriguez, J.A.; White, M.; Liu, P. Fundamental studies of methanol synthesis from CO_2 hydrogenation on Cu(111), Cu clusters, and Cu/ZnO(000$\bar{1}$), *Phys. Chem. Chem. Phys.* **2010**, *12* (16), 9909-9917.

TOC: